JOURNAL OF AIRCRAFT
Vol. 38, No. 4, July–August 2001

Control Surface Reversal in the Transonic Regime Including Viscous Effects

F. Eastep*
University of Dayton, Dayton, Ohio 45469
G. Andersen† and P. Beran‡
Air Force Research Laboratory, Wright–Patterson Air Force Base, Ohio 45433
and
R. Kolonay§
General Electric Corporate Research, Niskayuna, New York 12309

This paper investigates control surface reversal in the transonic flight regime. Surface-pressure distributions on a rigid and deformable wing are presented using linear and nonlinear aerodynamic methods, which incorporate the effects of surface shocks and viscosity with an interactive boundary layer. Transonic small-disturbance (TSD) aerodynamics is used to determine reversal of a typical fighter wing to study the interactions among control surface deflections, structural flexibility, and embedded shocks in a flowfield where significant viscous effects can exist. Pressure distributions on the wing are examined, and control surface reversal calculations are presented. The results show that the reduction of the reversal dynamic pressure can be as much as 30% when an aerodynamic method capable of representing a shock is used. A limited number of Euler computational fluid dynamic (CFD) results are presented for the purpose of comparison with transonic small disturbance results. The adequacy of using TSD theory in reversal prediction as compared to that obtained from either Euler or Navier–Stokes CFD aerodynamics is discussed. It is suggested that the inviscid transonic small disturbance aerodynamic provides a capability of representing shocks with only a modest increase of computer time beyond that necessary with the linear surface panel method. It is recommended that the inviscid version of TSD be incorporated in the preliminary design of aircraft operating at transonic speeds.

Nomenclature

A, B, E, F, G, H	=	coefficients in the transonic small disturbance equation
C_M	=	rolling-moment coefficient produced by aileron deflection
C_p	=	pressure coefficient
M_∞	=	freestream Mach number
γ	=	ratio of specific heats = 1.4
ΔC_p	=	surface-pressure coefficient differential
δ_a	=	aileron deflection
ε	=	control surface effectiveness
φ	=	small disturbance velocity potential

Subscripts

t	=	time differentiation
x, y, z	=	space differentiation

Introduction

TO perform structural design of flight vehicles, efficient and accurate maneuver loads predictions are required. Currently, there are many well-established techniques available to determine steady aerodynamic loads and static aeroelastic responses in subsonic and supersonic flight. These methods are also often used in the transonic region. Because these methods are based on linear aerodynamic theory, they are efficient but not considered accurate in this regime. The transonic flow condition is a mixture of subsonic and supersonic flow with embedded shocks; therefore, to accurately describe the transonic flowfield, nonlinear partial differential equations must be solved.

Until recently, little effort has been expended to include nonlinear aerodynamic loads in the preliminary structural design environment because of the large computational cost associated with the solution of the nonlinear equations. The inclusion of viscous effects demands even more resources. However, with advances in nonlinear aerodynamic flow solvers and computer hardware, nonlinear airloads including viscous effects are now available at computational costs that make the problem tractable.

The intent of this research is to develop an efficient and accurate analysis method that is capable of determining the aeroelastic response of a lifting surface with an articulated control surface in viscous and transonic flow. This method is then applied to the analysis of a simple fighter type wing to determine the significance of including viscous effects. Of particular interest is the control-surface effectiveness of a lifting surface in transonic flow. This study investigates the impact of including viscosity, aerodynamic nonlinearities, and structural flexibility in determining the control-surface reversal dynamic pressures.

Background

Aeroelastic analysis of flexible aircraft structures in the transonic flight regime is a relatively recent endeavor. In the late 1980s research was conducted in the prediction of steady and unsteady airloads in the transonic region through the use of classical transonic small-disturbance theory and the transonic full-potential equation.[1,2] Although both of these efforts included the effects of articulated control surfaces in the analysis, the effects of structural flexibility were not taken into account.

Currently, there is considerable interest in the U.S. Air Force in employing lightweight, reduced stiffness wing structures to affect maneuver performance. A rigid analysis is not sufficient in cases

Received 4 August 1999; revision received 15 December 2000; accepted for publication 12 January 2001.

*Professor, Mechanical and Aerospace Engineering. Associate Fellow AIAA.
†Aerospace Engineer, Capt. USAF. Member AIAA.
‡Senior Aerospace Engineer, Structural Design and Development Branch. Associate Fellow AIAA.
§Research Engineer, Structural Design and Development Branch. Associate Fellow AIAA.

where a flexible structure deforms under the generated airloads. This issue was addressed under an Air Force contract with Rockwell International.[3] The study considered the effects of structural flexibility under the influence of airloads created by a deflected control surface. Degradation of rolling moment with increased dynamic pressure was shown for a limited range of Mach numbers. However, an in-depth investigation into the effect of varying Mach number and the interaction between shocks and control surfaces was not undertaken.

In 1991 transonic small-disturbance theory was used to predict dynamic and steady aeroelastic phenomena concerning the F-15 and F/A-18 aircraft.[4] Although rolling-moment coefficients were not directly computed, prediction of control-surface reversal dynamic pressure was given at a single transonic Mach number based on examination of the behavior of the computed lift coefficient.

More recently, a study was undertaken that focused on a detailed examination of aeroelastic effects caused by control-surface deflections in transonic flow.[5] Emphasis was placed on accurate prediction of pressure distributions and steady aeroelastic phenomena. Rolling moments and control-surface reversal points were examined as the Mach number was varied from subsonic to supersonic values. It was discovered that inclusion of nonlinear aerodynamics significantly affected pressure distributions and steady aeroelastic behavior in the transonic regime.

The present study expands upon the previous paper (Ref. 5) by including the effects of a viscous boundary layer. Control-surface reversal dynamic pressures are calculated for both viscous and inviscid analyses, and the effects of including flow viscosity are considered.

Approach

Transonic Small-Disturbance Theory

Because flow in the transonic region is characterized by the occurance of surface shocks, the analyses in this regime must include a technique for describing accurately the shocks. The method employed in this study was transonic small-disturbance (TSD) theory. Although one of the simplest methods of nonlinear aerodynamics, TSD theory is capable of determining the strength and location of weak shocks, and because of its efficiency, it is generally considered appropriate for preliminary design.

The aeroelastic calculations were performed by the NASA Langley code CAP-TSD.[6] Using the finite difference method, the program solves the general frequency modified transonic small-disturbance potential equation, given here in differential form as

$$\frac{\partial f_0}{\partial t} + \frac{\partial f_1}{\partial x} + \frac{\partial f_2}{\partial y} + \frac{\partial f_3}{\partial z} = 0 \tag{1}$$

where

$$f_0 = -A\phi_t - B\phi_x, \qquad f_1 = E\phi_x + F\phi_x^2 + G\phi_y^2$$
$$f_2 = \phi_y + H\phi_x\phi_y, \qquad f_3 = \phi_z \tag{2}$$

The coefficients A, B, and E are defined as

$$A = M_\infty^2, \qquad B = 2M_\infty^2, \qquad E = 1 - M_\infty^2 \tag{3}$$

Within CAP-TSD there are a number of options for specifying the coefficients F, G, and H, depending upon the assumptions used in deriving the transonic small-disturbance equation. For the nonlinear analyses the coefficients are

$$F = -\tfrac{1}{2}(\gamma + 1)M_\infty^2, \qquad G = -\tfrac{1}{2}(\gamma - 3)M_\infty^2, \qquad H = -M_\infty^2 \tag{4}$$

and for the linear cases

$$F = G = H = 0 \tag{5}$$

Viscous Effects

The effects of viscosity are included through the modeling of a viscous boundary layer on a flat plate. Solution of the lag-entrainment boundary-layer equations yields the momentum thickness, shape factor, and entrainment coefficient for the boundary layer as a function of distance along the chord.

Within CAP-TSD the solution technique is based upon the implementation by Howlett of interactive boundary-layer modeling (IBLM).[7] IBLM treats the complete dynamic system as two coupled portions, the outer inviscid flow and the inner viscous flow. The amount of coupling error between the two systems is minimized as the edge velocities of the inner-flow and outer-flow regions are matched.

In general, both attached and separated boundary-layer flows are treated through an inverse solution scheme. This is necessary as the boundary-layer equations become singular when the flow separates.

It is beyond the scope of this work to fully describe the development of the viscous CAP-TSD code, CAP-TSDV, or the numerical solution of the boundary-layer equations. For further description Ref. 8 should be consulted.

Euler Computational Fluid Dynamics

To compare inviscid CAP-TSD results with a higher-order computational fluid dynamics (CFD) code, a number of Euler CFD runs were made with the ENS3DAE (Euler/Navier–Stokes Three-Dimensional Aeroelastic) CFD software. Like CAP-TSD, ENS3DAE is a method for the computation of inviscid and viscous flows about flexible aircraft structures. The CFD method is a central difference, multiblock, approximate factorization algorithm for the implicit time integration of the Euler or Navier–Stokes equations. It is second-order accurate in both space and time. ENS3DAE has been extensively applied and modified since its delivery to Air Force Wright Laboratory (now Air Force Research Laboratory, Air Vehicles Directorate) by the then Lockheed Aeronautical Systems Company. Further details of the methodology, including applications to practical configurations, are provided in Refs. 9–11.

Steady Aeroelastic Analysis

Aeroelastic analyses in CAP-TSD and ENS3DAE are carried out in generalized modal coordinates. Required mode shapes were obtained through an eigenvalue analysis in which the stiffness and mass of the system were represented by the finite element method. Structural eigenvalues, eigenvectors, and generalized mass and stiffness were determined using the Automated Structural Optimization System.[12] The structural eigenvectors were then splined to the aerodynamic degrees of freedom, represented by the CAP-TSD or ENS3DAE computational mesh, using the infinite-plate spline.[13] With the splined mode shapes and generalized mass and stiffness the static aeroelastic analysis was performed using appropriate boundary conditions in CAP-TSD or ENS3DAE. These analyses yielded the velocity potentials and pressure coefficients at the computational mesh modes. Finally, the pressure coefficients were integrated to obtain the necessary aerodynamic coefficients and stability derivatives.

Because steady-state roll performance was the subject of this study, an appropriate rolling maneuver performance parameter was employed. Control-surface effectiveness ε is given by the following:

$$\varepsilon = \frac{C_{M_{\delta a\,\text{flexible}}}}{C_{M_{\delta a\,\text{rigid}}}} \tag{6}$$

where the numerator and denominator are respectively the flexible and rigid derivatives of the rolling-moment coefficients with respect to control-surface deflection at a given flight condition. Assuming a constant angle of attack, control-surface deflection, and Reynolds number, the rigid rolling-moment coefficient varies with Mach number only. For the aeroelastic condition this coefficient varies with Mach number and dynamic pressure as structural flexibility is included in the analysis.

A steady aeroelastic phenomenon of interest, control-surface reversal, occurs when ε becomes zero. Determination of control-surface effectiveness at various Mach numbers and dynamic pressures yields the control surface reversal points. A plot of ε against dynamic pressure gives the reversal point for a particular Mach number. This procedure can be carried out for both viscous and inviscid analyses. Doing so allows the significance of viscous effects in the prediction of control-surface effectiveness and reversal points to be quantified.

Analysis Model

This analysis procedure was carried out on a model of a generic fighter type aircraft, taken from Ref. 14. The structural model of the wing was a fully built-up finite element model with a stiffness representative of stiff, low-aspect-ratio fighter wing. A NACA 0004 airfoil was used to represent the wing thickness. A single inboard trailing-edge control surface, or flaperon, was utilized. The full TSD computational mesh for this model was a $154 \times 46 \times 80$ grid (chord $\times$ normal $\times$ span). One-hundred chordwise and 23 spanwise grid points were used on the aerodynamic surface. The planform geometry and CAP-TSD aerodynamic mesh of this wing are depicted in Fig. 1.

For the ENS3DAE analysis of the thin wing in this study, a two-zone H-H grid topology is used. A planform view of the grid is shown in Fig. 2. Each zone is comprised of 120 points in the streamwise direction, 50 points normal to the wing, and 59 spanwise points, leading to a complete grid of 708,000 points. On the wing surface 61 points are distributed in the streamwise direction and 45 in the spanwise direction. Grid-point clustering is maintained along the flaperon hinge line and along the leading and trailing edges. Dimensions of the computational domain are identical to those specified for the CAP-TSD analysis. This aeroelastic definition has the advantage of providing structural modeling consistency between CAP-TSD and ENS3DAE.

The finite element model of the wing structure consisting of 10 spars and 4 ribs is shown in Fig. 3.

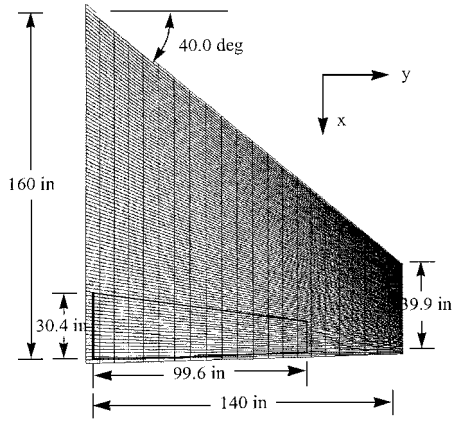

Fig. 1 Fighter wing planform and CAP-TSD small-disturbance mesh.

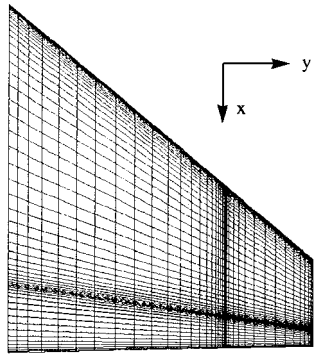

Fig. 2 ENS3DAE Euler computational mesh.

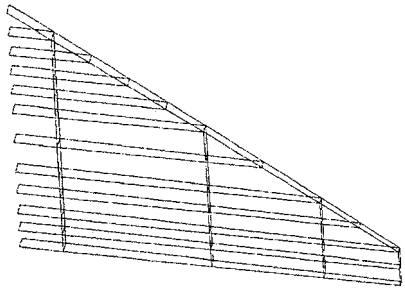

Fig. 3 Fighter wing finite element model.

Results

CAP-TSD Analyses

Three types of analyses were performed on the wing model. For baseline comparison a linear inviscid analysis was performed. A nonlinear inviscid analysis was then performed to determine changes in pressure distribution caused by nonlinear aerodynamics. Finally, a complete nonlinear viscous analysis was performed to observe the effects of a viscous boundary layer. These analyses were done over a range of Mach numbers varying from 0.70 to 0.97. Both rigid and flexible analyses were performed to illustrate the effects of structural flexibility in the transonic regime.

To gain a basic understanding of the aerodynamics associated with shock and viscous effects without the influence of structural flexibility, rigid analyses were first performed, and resultant pressure coefficient distributions were computed. Results for these analyses are shown in Figs. 4–6 for Mach numbers of 0.70, 0.94, and 0.96. At Mach 0.70, as Figs. 4a–4c illustrate, there were few qualitative differences among the results of the three analyses. As expected, no shocks developed on the wing at this subsonic Mach number, resulting in little difference between the linear inviscid and nonlinear inviscid analyses (Figs. 4a and 4b).

Results of the nonlinear inviscid and nonlinear viscous analyses are presented in Figs. 4b and 4c. At this flow condition qualitative differences between the two cases are again minor. Quantitatively, the effects of viscosity lead to a decrease in the magnitude of the pressure spike at the control-surface hinge line.

Flow nonlinearities become significant at higher Mach numbers. This is illustrated at Mach 0.94 in Figs. 5a–5c. In the linear analysis (Fig. 5a) the only pressure rise predicted is at the control-surface hinge line. When nonlinear aerodynamics are included, however, a second pressure rise is generated (Fig. 5b). At this transonic Mach number shocks form on both upper and lower surfaces of the wing upstream of the control surface hinge line. Because of the deflection of the control surface, the positions of the shocks are altered so that the shock on the upper surface is further downstream than the shock on the lower surface.

At this transonic Mach number the effects of viscosity are included and result in a general chordwise smoothing (reduction in shock strength) of the pressure field (Fig. 5c). As with the case at Mach 0.70, the magnitude of the pressure spike at the hinge line is reduced. In this case, though, the difference is greater. Furthermore, the pressure rise in the region of the shocks is also reduced as viscous effects near the shocks are taken into account.

At a slightly higher Mach number of 0.96, the differences between the linear and nonlinear analyses remain significant (Figs. 6a and 6b). Again, shocks form on the surface of the wing and dramatically change the pressure field when aerodynamic nonlinearities are included. At this Mach number the location of the shocks are shifted downstream, and the shock on the upper surface now falls aft of the control-surface hinge line.

When viscous effects are included (Fig. 6c), the effects are even more significant than those seen at the lower Mach numbers. As with the prior cases, the general trend is a lowering of the magnitude of the pressure rises in the region of the shocks and at the control-surface hinge line. The smoothing of the pressure field is significant and results in lower chordwise pressure gradients than predicted by the inviscid analysis.

Structural flexibility was included in the analyses at Mach 0.94. The resultant pressure coefficient distributions are shown in Figs. 7a–7c. The consequences of a flexible structure become evident as the leading edge of the wing twists downward in response to the pressure rises aft of the structural elastic axis. This leads to negative resultant pressures near the leading edge. At a certain dynamic pressure the result is control-surface reversal, the point at which a control surface is completely ineffective at generating a rolling moment.

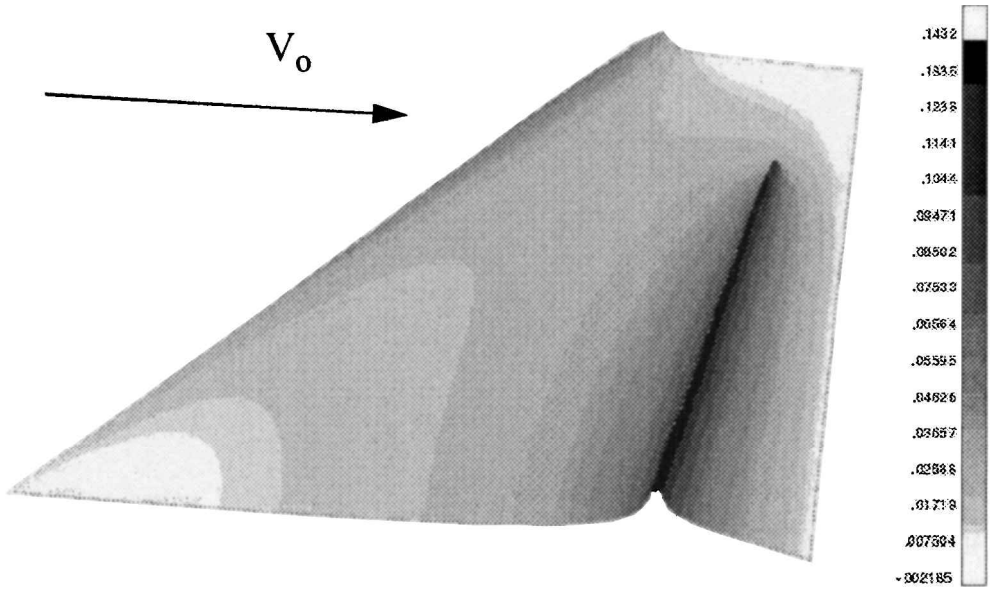

Fig. 4a CAP-TSD rigid linear inviscid resultant pressure coefficient distribution at Mach 0.70.

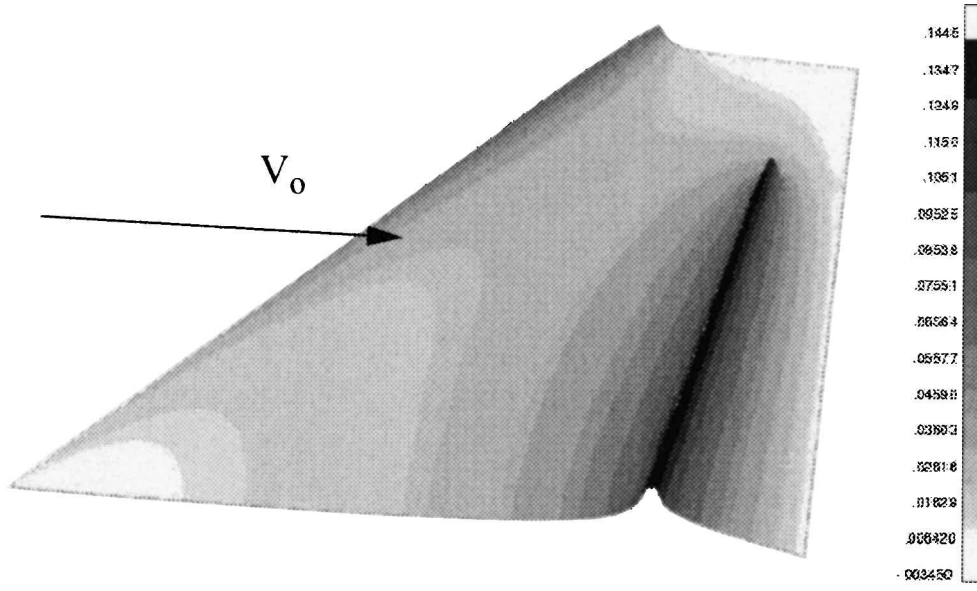

Fig. 4b CAP-TSD rigid nonlinear inviscid resultant pressure coefficient distribution at Mach 0.70.

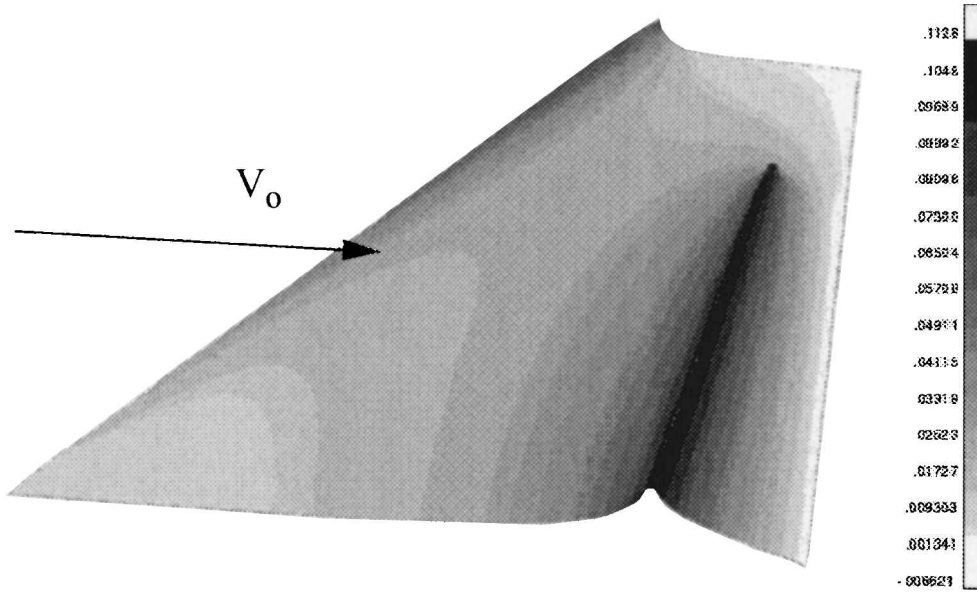

Fig. 4c CAP-TSD rigid nonlinear viscous resultant pressure coefficient distribution at Mach 0.70.

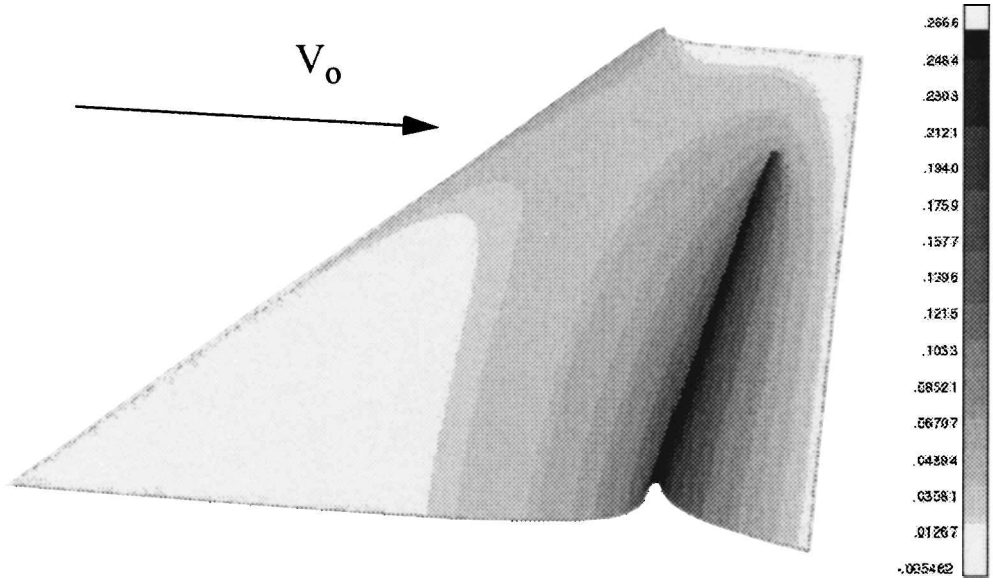

Fig. 5a CAP-TSD rigid linear inviscid resultant pressure coefficient distribution at Mach 0.94.

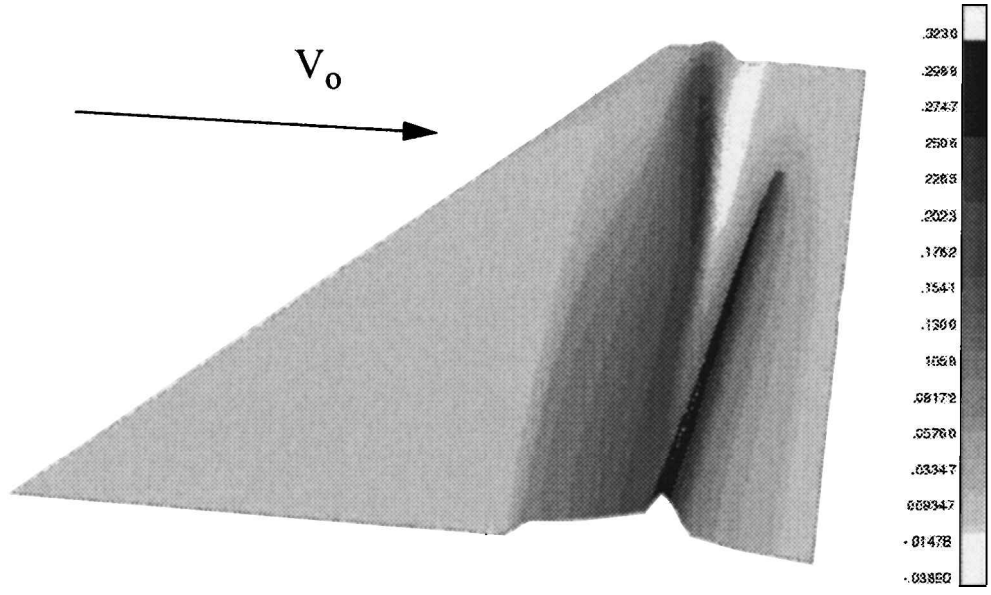

Fig. 5b CAP-TSD rigid nonlinear inviscid resultant pressure coefficient distribution at Mach 0.94.

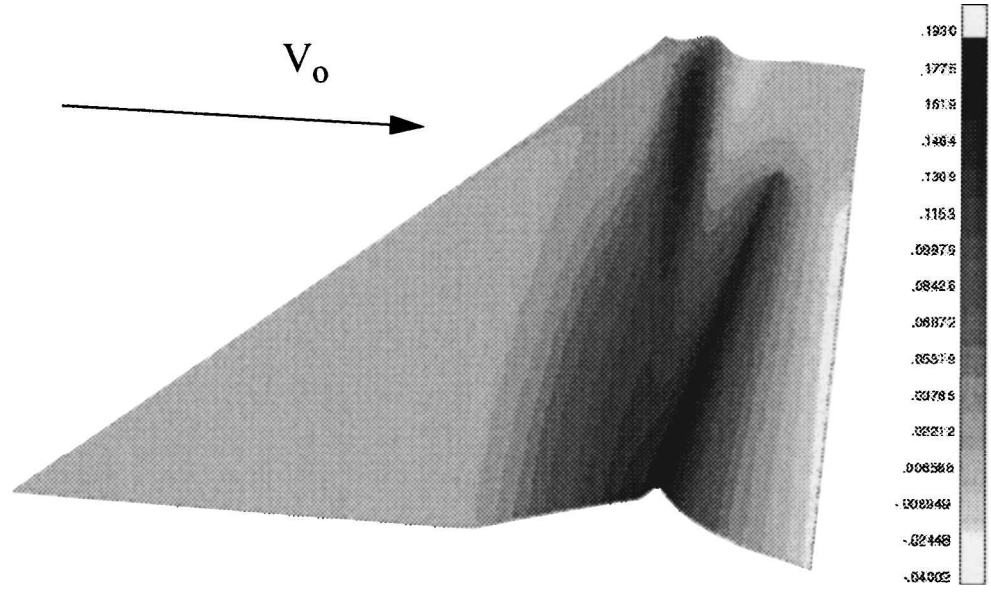

Fig. 5c CAP-TSD rigid nonlinear viscous resultant pressure coefficient distribution at Mach 0.94.

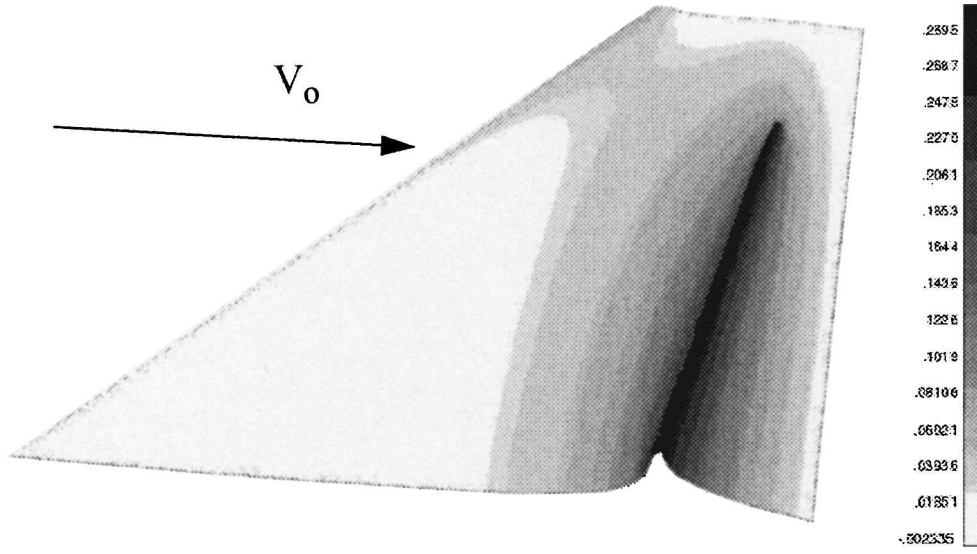

Fig. 6a CAP-TSD rigid linear inviscid resultant pressure coefficient distribution at Mach 0.96.

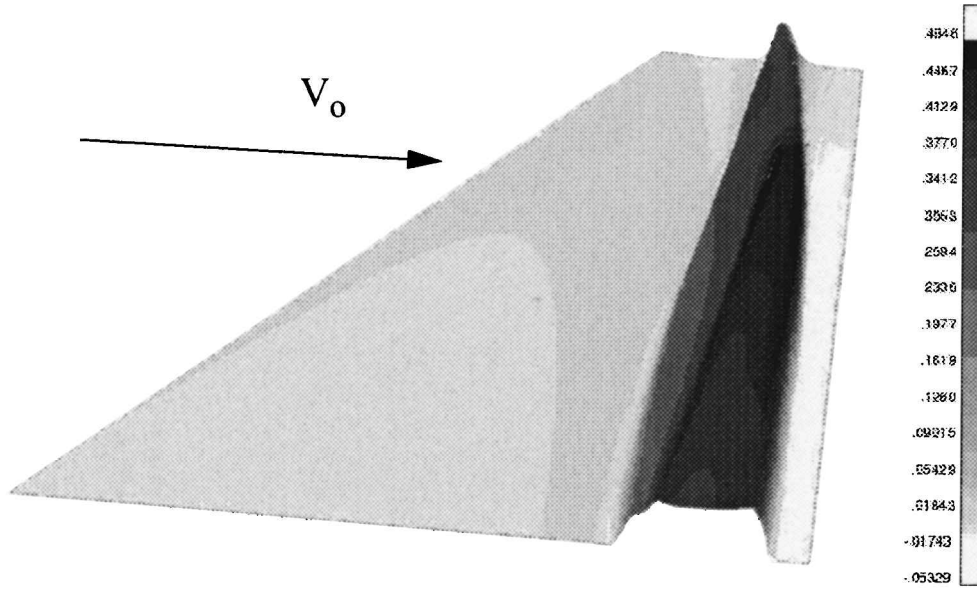

Fig. 6b CAP-TSD rigid nonlinear inviscid resultant pressure coefficient distribution at Mach 0.96.

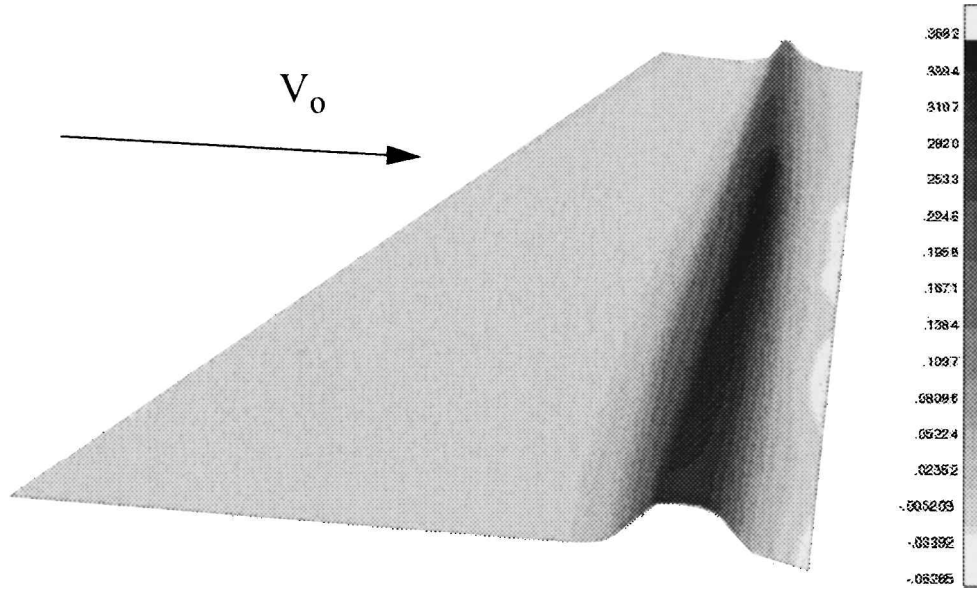

Fig. 6c CAP-TSD rigid nonlinear viscous resultant pressure coefficient distribution at Mach 0.96.

For the linear inviscid case the only adverse twisting of the wing is caused by the pressure rise at the control-surface hinge line (Fig. 7a). In the nonlinear case there is a second contribution caused by the pressure rise in the region of the shocks as seen in Fig. 7b. This leads to a greater twisting of the wing and, consequently, lower reversal dynamic pressures.

Inclusion of viscous effects (Fig. 7c), as seen in the rigid analyses, leads to a general reduction in the magnitude of pressure rises. This effectively lessens the moment acting to twist the wing. As a result, inclusion of viscosity in this study generated higher reversal dynamic pressures than predicted by an inviscid analysis.

Comparison of TSD and Euler Analyses

An important aspect of this work is the determination of the adequacy of TSD theory in predicting the pressure distribution on a lifting surface with a deflected control surface in transonic flow. To gain some insight into this issue, a number of ENS3DAE analyses were made so that the CAP-TSD (nonlinear, inviscid) results could be compared against the higher-order results generated by Euler CFD.

The first of these comparisons is presented in Fig. 8. The plot shows a chordwise pressure coefficient distribution predicted by CAP-TSD and ENS3DAE for the rigid case at a subsonic Mach

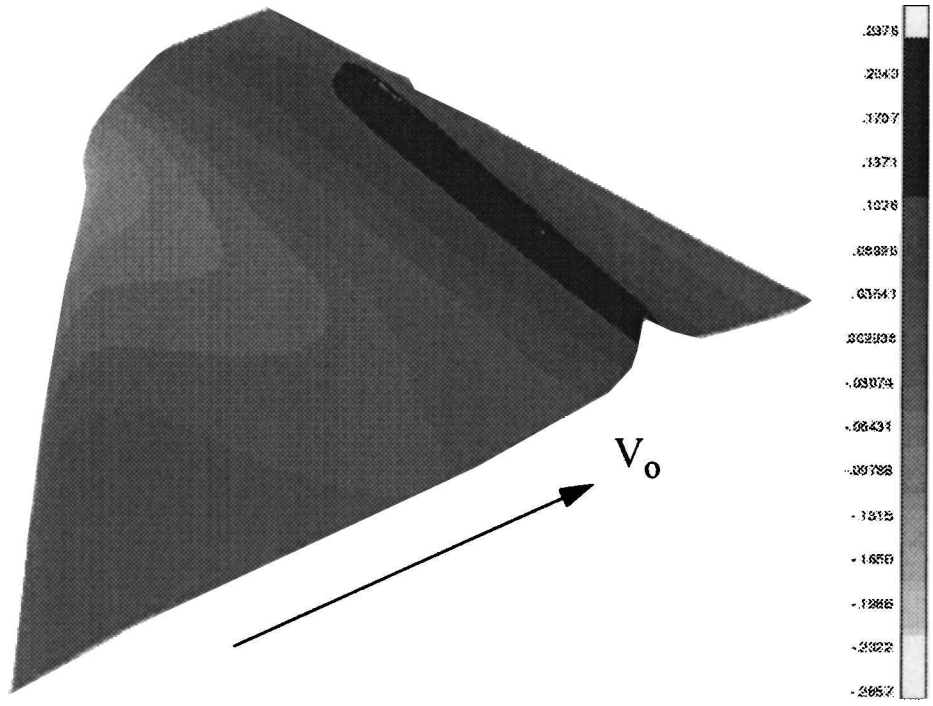

Fig. 7a CAP-TSD aeroelastic linear inviscid resultant pressure coefficient distribution at Mach 0.94.

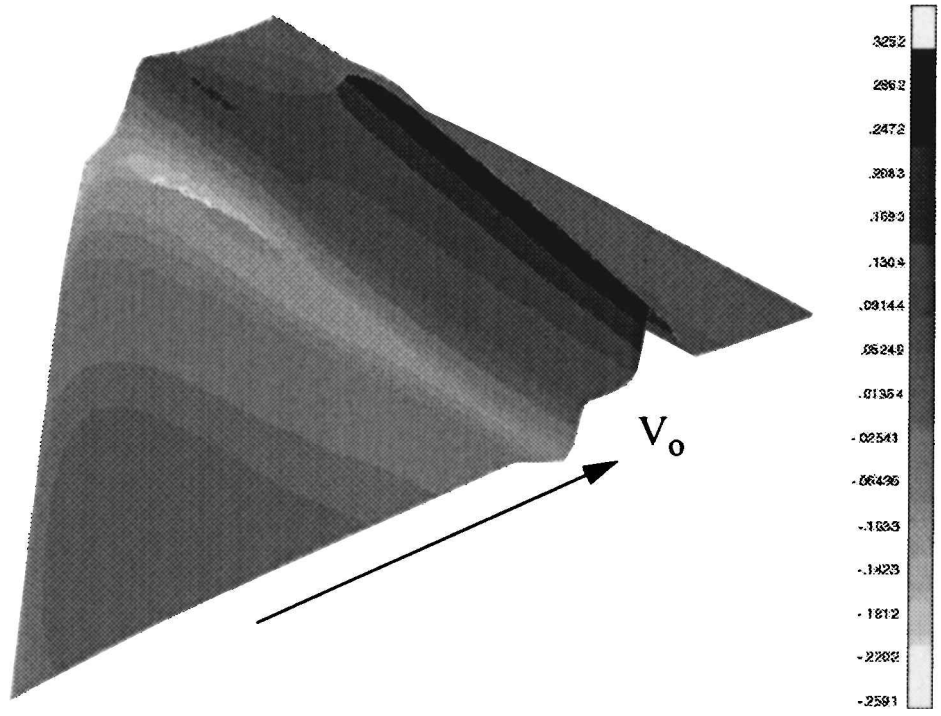

Fig. 7b CAP-TSD aeroelastic nonlinear inviscid resultant pressure coefficient distribution at Mach 0.94.

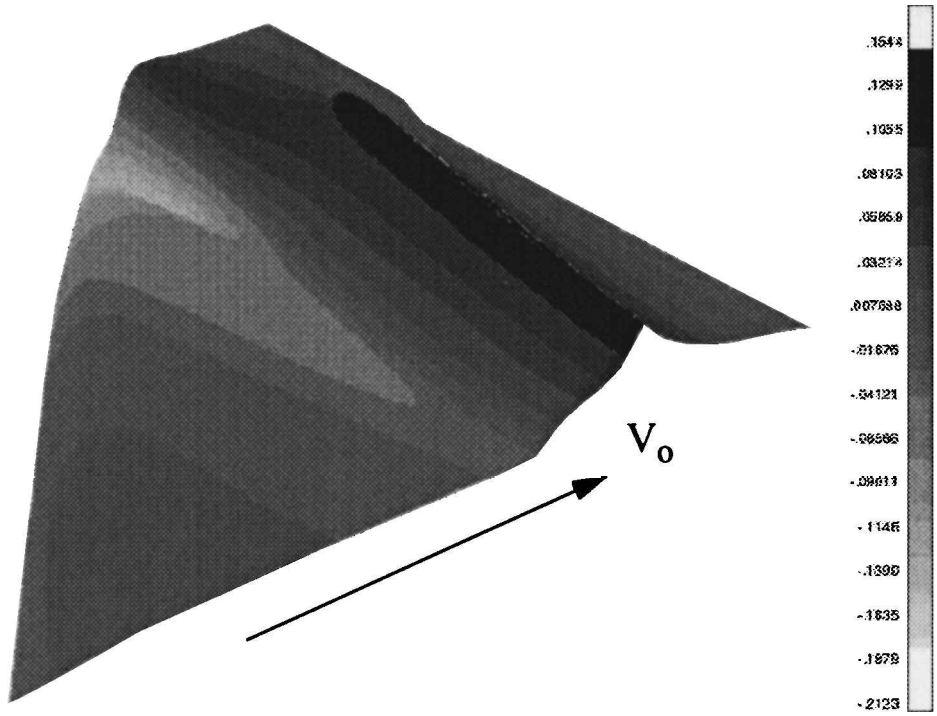

Fig. 7c CAP-TSD aeroelastic nonlinear viscous resultant pressure coefficient distribution at Mach 0.94.

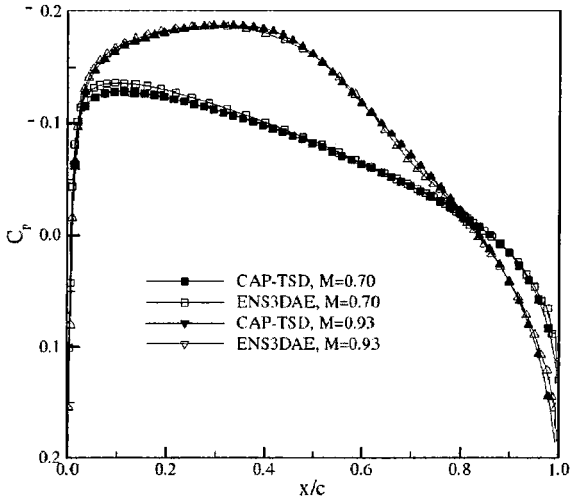

Fig. 8 Chordwise rigid pressure coefficient distribution for no-control-surface deflection.

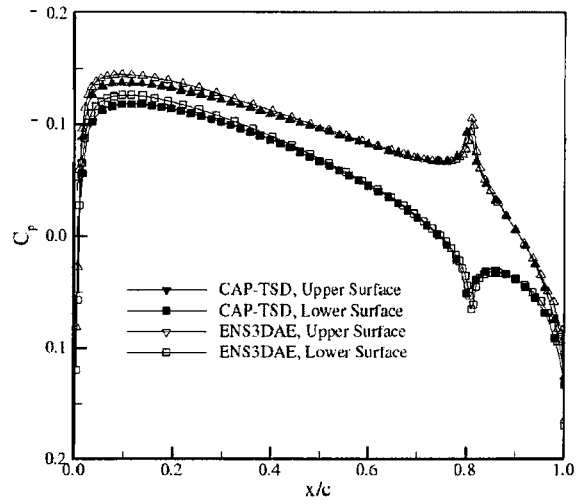

Fig. 9 Chordwise rigid pressure coefficient distribution for 1-deg control-surface deflection at Mach 0.70.

number of 0.70 and a transonic Mach number of 0.93. The spanwise station is at approximately the midspan of the control surface. To obtain a baseline comparison, the control surface was not deflected. At this symmetric condition the upper and lower surface-pressure coefficients collapse to the same values. The results generated by the two codes are in close agreement.

The next comparison concerned the prediction of the pressures generated at the control-surface hinge line caused by a one-deg downward control-surface deflection. The results for a rigid subsonic analysis at Mach 0.70 are shown in Fig. 9. Again, the predicted pressure distributions are in close agreement for both upper and lower surfaces. The rolling-moment coefficients are in agreement within 15% with a value of 0.0127 predicted by CAP-TSD and 0.0108 by ENS3DAE.

The same analysis for a one-deg control-surface deflection was performed at a Mach number of 0.94. The upper and lower surface pressure coefficients for this case are plotted in Fig. 10. At this transonic Mach number there is a clear discrepancy between the CAP-TSD and ENS3DAE results in the prediction of the strength and location of the shocks on the surface of the wing. This results in

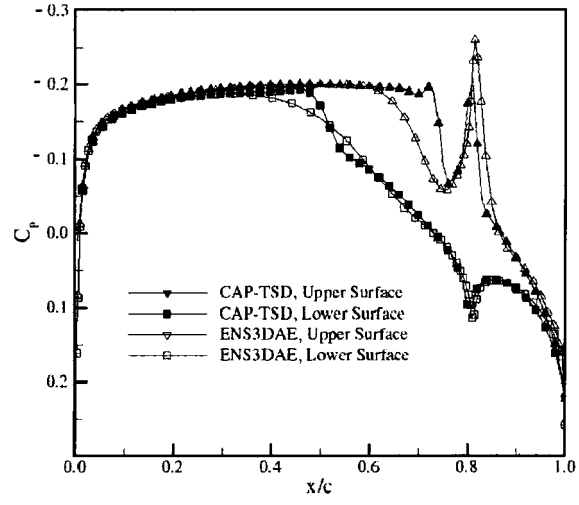

Fig. 10 Chordwise rigid pressure coefficient distribution for 1-deg control-surface deflection at Mach 0.94.

a significant difference in the calculated rigid rolling-moment coefficient. CAP-TSD yielded a value of 0.0200, whereas ENS3DAE predicted a value of 0.0157. The difference in shock location and strength remains significant for the flexible condition as shown in Fig. 11.

To obtain a clearer qualitative comparison between CAP-TSD and ENS3DAE results, three-dimensional carpet plots of the pressure coefficient distribution caused by a one-deg control-surface deflection were generated for the rigid case using both codes. The results at Mach 0.70 are shown in Figs. 12a and 12b. The corresponding results for Mach 0.94 are illustrated in Figs. 13a and 13b. As seen in the preceding chordwise pressure plots, the results from the codes agree well for the subsonic case. At the transonic Mach number, however, a difference in the pressure rise in the region of the shocks is apparent.

The influence of aerodynamic nonlinearities and flow viscosity on the variation of reversal dynamic pressure with Mach number is shown in Fig. 14. In addition to trend results generated by CAP-TSD, reversal points at Mach 0.93, 0.94, 0.95, and 0.96 were calculated using ENS3DAE and are also shown in Fig. 14. Consistent with the observations made from the resultant pressure distributions predicted by CAP-TSD, the nonlinear inviscid reversal dynamic pressures are lower than the linear inviscid reversal pressures. The nonlinear viscous reversal dynamic pressures are approximately 10% higher than the nonlinear inviscid results and are in fact higher than the linear inviscid reversal pressures except at Mach numbers beyond 0.96.

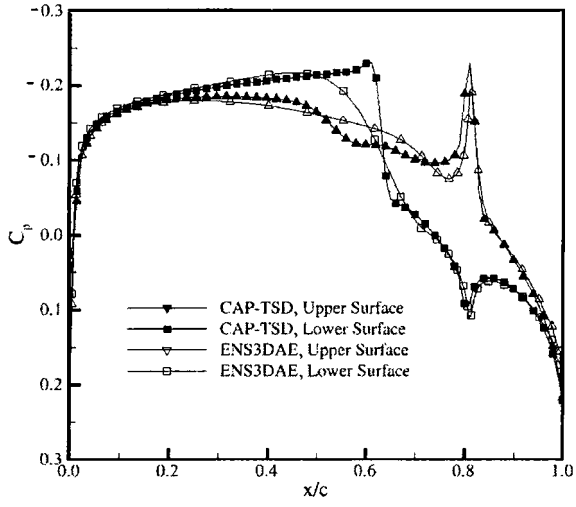

Fig. 11 Chordwise aeroelastic pressure coefficient distribution for 1-deg control-surface deflection at Mach 0.94.

Assessment of Computer Requirements

The goal of this investigation is to develop efficient and accurate aerodynamic methods capable of determining control-surface reversal in the transonic regime. Further, the aerodynamic methods are to be used in a preliminary design environment where many analyses are required, and the computer time for a single analysis must be kept at a minimum. The computer time required for the prediction of control surface reversal with various aerodynamic methods is shown in Table 1. The time shown in Table 1 represents the normal time required for reversal determination as computed on an SGI-Octane workstation.

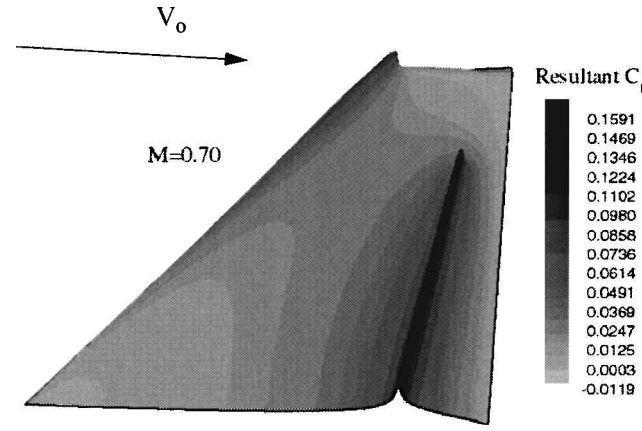

Fig. 12b ENS3DAE resultant rigid pressure coefficient distibution at Mach 0.70.

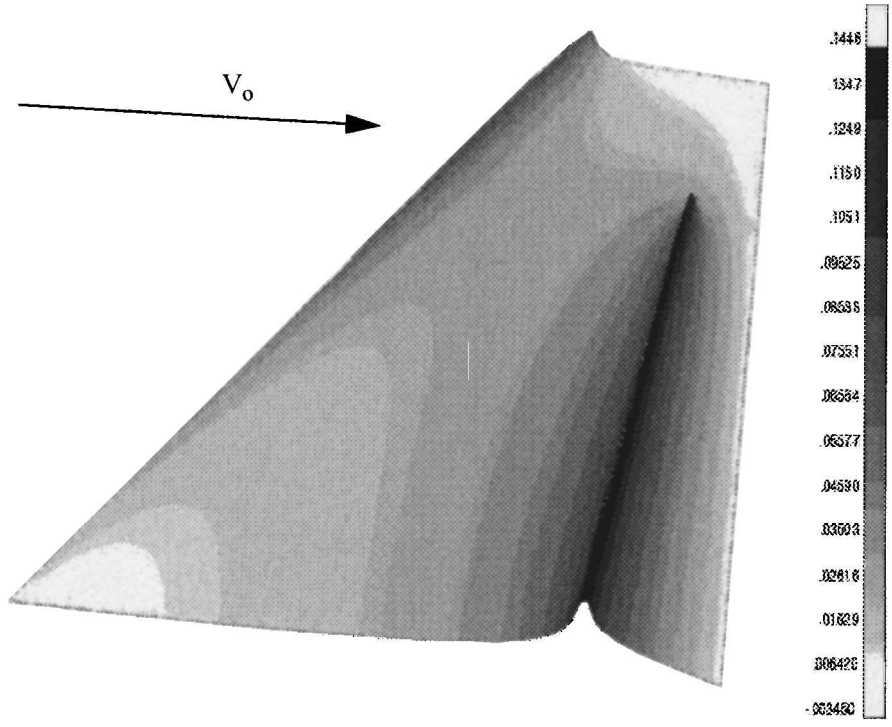

Fig. 12a CAP-TSD resultant pressure coefficient distribution at Mach 0.70.

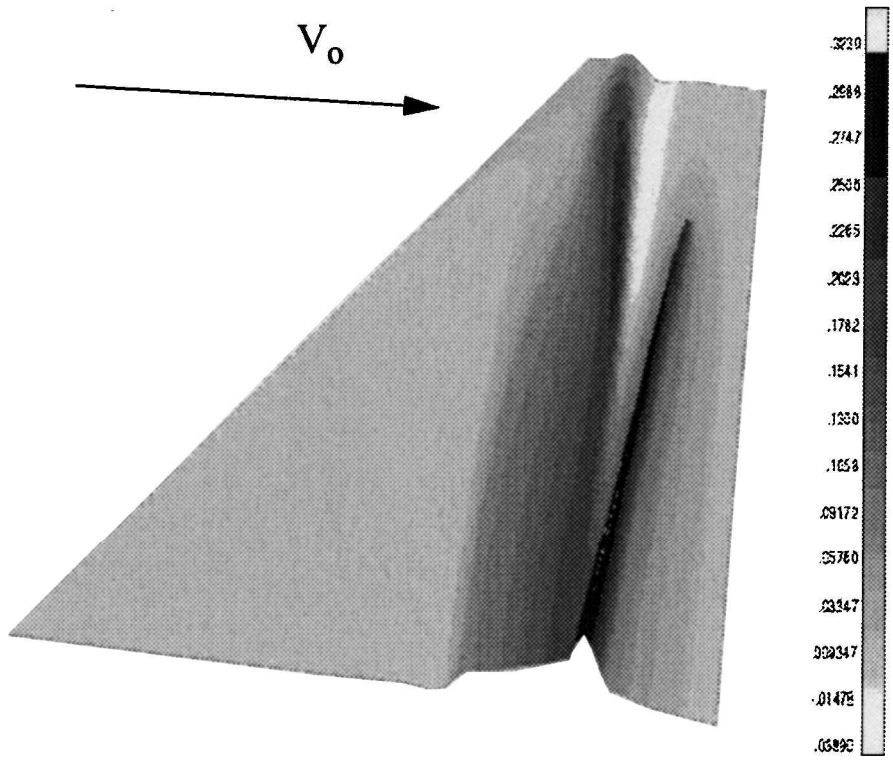

Fig. 13a CAP-TSD resultant rigid pressure coefficient distribution at Mach 0.94.

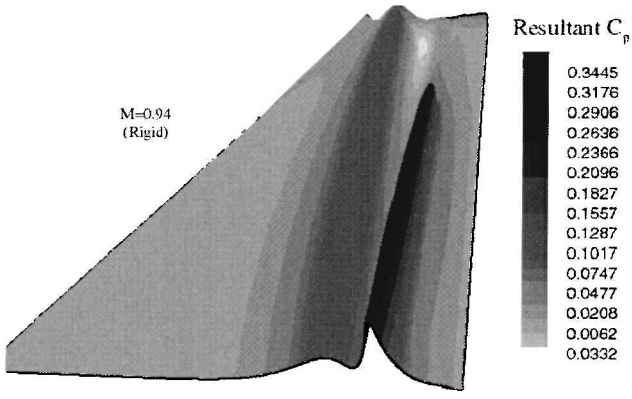

Fig. 13b ENS3DAE resultant rigid pressure distribution at Mach 0.94.

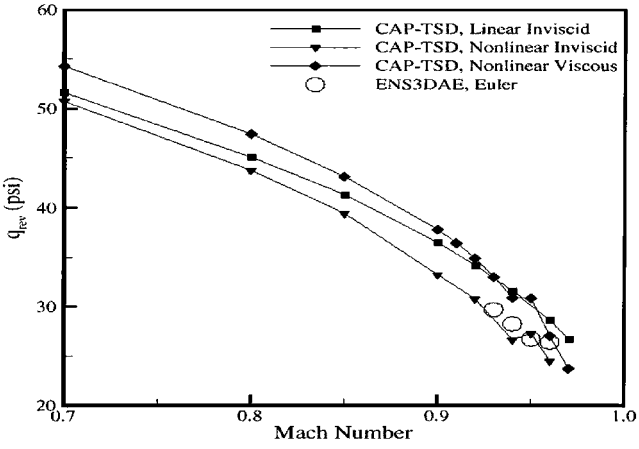

Fig. 14 Control-surface reversal dynamic.

Table 1 Time required for reversal determination

Aerodynamic method	Time, h[a]
Linear (surface paneling)	0.1
Inviscid linear (CAP-TSD)	1.0
Inviscid nonlinear (CAP-TSD)	1.2
Viscous nonlinear (CAP-TSDV)	20
Inviscid nonlinear (Euler)	20
Viscous nonlinear (Navier–Stokes)	50

[a]Time as computed on a SGI-Octane workstation.

As shown in Table 1, the linear surface paneling method yields the least time requirement and is a well-established technique used in preliminary design. But the paneling and the inviscid, linear CAP-TSD, requiring 10 times the time necessary for the paneling methods, are not accurate in the transonic regime because of the inability of representing surface shocks. The nonlinear inviscid CAP-TSD does represent surface shocks but with an increase of computing time of 12 times the paneling method time. The nonlinear, viscous CAP-TSDV and the inviscid, nonlinear Euler methods both represent surface shocks but require 200 times as much computing time as does the paneling method. The nonlinear, viscous Navier–Stokes represents an increase of computer time by 500 times beyond that necessary for the paneling method.

It appears from Table 1 that the nonlinear, inviscid CAP-TSD does provide a capability of representing surface shocks with a modest increase of computing time beyond the time required for the paneling method. The increase of computing times seems to be an acceptable cost when this aerodynamic prediction method is included in the preliminary design of vehicles operating at transonic speeds.

Conclusions

The aeroelastic analyses of the wing model demonstrates that the presence of viscosity has an impact on the steady aeroelastic characteristics of the wing. Examination of pressure distributions indicates that viscous effects reduce the magnitude of the resultant pressure rise in the region of the wing aft of the structural

elastic axis. This serves to delay control-surface reversal and increases the dynamic pressure at which this aeroelastic phenomena occurs.

Because the overall objective of this research is to develop analysis techniques suitable for preliminary design of aircraft structures, the findings of this research should be viewed in this context. The results of this study indicate that it would not necessarily be beneficial to use a viscous analysis over the entire transonic regime to determine structural loadings for design purposes. As in the case considered in this work, use of the nonlinear inviscid results would result in a more conservative design without resorting to expensive viscous analyses.

The results of this research are considered preliminary and by no means exhaustive. During this study, separated flow was not encountered; therefore, no observations can yet be made concerning the impact of separated flow on reversal dynamic pressure. Furthermore, the upper Mach number explored was 0.97. Beyond this, stable solutions were not obtained. Until a more complete picture of the reversal behavior in the complete transonic regime can be completed, it would be premature to suggest that viscous effects need never be accounted for in the preliminary design of aircraft structures subject to transonic flow conditions.

To gain a more complete understanding of the influence of viscosity on steady aeroelastic phenomena, further research needs to be conducted. As already stated, effects of viscosity should be explored over the complete transonic regime. Separated flow, particularly at the base of the shocks should also be investigated. Navier–Stokes CFD analyses should be made in ENS3DAE to correlate the effects of viscosity predicted with this higher fidelity scheme to those obtained from transonic small-disturbance theory with boundary-layer corrections.

Acknowledgments

The authors wish to recognize Maj. Brian Sanders of the Air Force Office of Scientific Research. Major Sanders is responsible for the funding support of this research.

The authors also wish to acknowledge the Major Shared Resource Centers at Aeronautical Systems Center, Wright–Patterson Air Force Base, Ohio, and Army Research Lab. located at Aberdeen Proving Ground, Maryland. These high-performance computing centers provided the computational hardware used in this research.

References

[1] Sotamayer, W. A., "Unsteady Transonic Flow for a Wing with Control Surface Deflections," U.S. Air Force Wright Aeronautical Lab., AFWAL TM-86-186-FIBR, Dayton, OH, Jan. 1987.

[2] Bharadvaj, B. K., "Computation of Steady and Unsteady Control Surface Loads in Transonic Flow," *Proceedings of the AIAA/ASME/ASCE/AHS/ASC 31st Structures, Structural Dynamics and Materials Conference*, AIAA, Washington, DC, 1990, pp. 1349–1360.

[3] Miller, G. D., "Active Flexible Wing (AFW) Technology," U.S. Air Force Wright Aeronautical Lab., AFWAL TR-87-3096, Dayton, OH, Feb. 1988.

[4] Pitt, D. M., and Fuglsang, D. F., "Aeroelastic Calculations for Fighter Aircraft Using the Transonic Small Disturbance Equation," AGARD CP 507 Transonic Unsteady Aerodynamics and Aeroelasticity, AGARD, Neuilly-sur-Seine, France, 1992, pp. 16-1–16-11.

[5] Andersen, G. R., Kolonay, R. M., and Eastep, F. E., "Control Surface Reversal in the Transonic Regime," *Journal of Aircraft*, Vol. 35, No. 5, 1998, pp. 688–694.

[6] Batina, J. T., "A Finite-Difference Approximate-Factorization Algorithm for Solution of the Unsteady Transonic Small-Disturbance Equation," NASA TP 3129, Jan. 1992.

[7] Howlett, J. T., "Efficient Self-Consistent Viscous Inviscid Solution for Unsteady Transonic Flow," *Journal of Aircraft*, Vol. 24, No. 11, 1987, pp. 737–744.

[8] Edwards, J. W., "Transonic Shock Oscillations and Wing Flutter Calculated with an Interactive Boundary Layer Coupling Method," NASA TM 110284, Aug. 1996.

[9] Schuster, D. M., Vadyak, J., and Atta, E., "Static Aeroelastic Analysis of Fighter Aircraft Using a Three-Dimensional Navier–Stokes Algorithm," *Journal of Aircraft*, Vol. 27, No. 9, 1990, pp. 820–825.

[10] Schuster, D. M., "Application of Navier–Stokes Aeroelastic Methods to Improve Fighter Wing Performance," *Journal of Aircraft*, Vol. 32, No. 1, 1995, pp. 77–83.

[11] Schuster, D. M., Beran, P. S., and Huttsell, L. J., "Application of the ENS3DAE Euler/Navier–Stokes Aeroelastic Method," AGARD CP 822 Numerical Unsteady Aerodynamic and Aeroelastic Simulation, AGARD, Neuilly-sur-Seine, France, 1997, pp. 3-1–3-11.

[12] Johnson, E. H., and Venkayya, V. B., "Automated Structural Optimization System (ASTROS)," Vol. 1, Theoretical Manual, U.S. Air Force Wright Aeronautical Lab., AFWAL TR-88-3028, Daylon, OH, Dec. 1988.

[13] Harter, R. L., and Desmarais, R. N., "Interpolation Using Surface Splines," *Journal of Aircraft*, Vol. 9, No. 2, 1972, pp. 189–191.

[14] Bishop, J. A., Eastep, F. E., Striz, A. G., and Venkayya, V. B., "Influence of Model Complexity and Aeroelastic Constraints on Multidisciplinary Optimization of Wings," *Journal of Aircraft*, Vol. 35, No. 5, 1998, pp. 784–790.